

## Research Article

# Smart Tendon Actuated Flexible Actuator

**Md. Masum Billah and Raisuddin Khan**

*Department of Mechatronics Engineering, Faculty of Engineering, International Islamic University Malaysia, 53100 Kuala Lumpur, Malaysia*

Correspondence should be addressed to Md. Masum Billah; [masum.uia@gmail.com](mailto:masum.uia@gmail.com)

Received 4 November 2014; Accepted 1 January 2015

Academic Editor: Gordon R. Pennock

Copyright © 2015 Md. M. Billah and R. Khan. This is an open access article distributed under the Creative Commons Attribution License, which permits unrestricted use, distribution, and reproduction in any medium, provided the original work is properly cited.

We investigate the kinematic feasibility of a tendon-based flexible parallel platform actuator. Much of the research on tendon-driven Stewart platforms is devoted either to the completely restrained positioning mechanism (CRPM) or to one particular type of the incompletely restrained positioning mechanism (IRPM) where the external force is provided by the gravitational pull on the platform such as in cable-suspended Stewart platforms. An IRPM-based platform is proposed which uses the external force provided by a compliant member. The compliant central column allows the configuration to achieve  $n$  DOFs with  $n$  tendons. In particular, this investigation focuses on the angular deflection of the upper platform with respect to the lower platform. The application here is aimed at developing a linkable module that can be connected to one another so as to form a “snake robot” of sorts. Since locomotion takes precedence over positioning in this application, a 3-DOF Stewart platform is adopted. For an arbitrary angular displacement of the end-effector, the corresponding length of each tendon can be determined through inverse kinematics. Mathematical singularities are investigated using the traditional analytical method of defining the Jacobian.

## 1. Introduction

In this research we have designed and developed a smart material actuated tendon-based flexible single link actuator. The smart material used in this project is called electroactive polymer (EAP). This actuator is a special version of a Stewart platform developed as a small-scale tendon-driven flexible actuator. Much of the research on tendon-driven Stewart platforms is devoted either to the completely restrained positioning mechanism (CRPM) or to one particular type of the incompletely restrained positioning mechanism (IRPM) where the external force is provided by the gravitational pull on the platform such as in cable-suspended Stewart platforms. The actuator developed here is based on IRPM. It uses a central compliant member connecting two parallel platforms while the two platforms are connected by three active tendons placed at the outer edges of the platforms. The tendons are parallel to the central compliant member while none of the tendons are activated. The compliant central column allows the configuration to achieve 3 DOFs with different activation (force) of the 3 tendons. In particular, this investigation focuses on the angular displacement between the two

platforms. This actuator has lots of applications in systems where ball-and-socket joints are used. The application here is aimed at developing a linkable module that can be connected to one another so as to form a 3-DOF “snake robot” of sorts. For an arbitrary angular displacement between two platforms, the corresponding length of each tendon can be determined through inverse kinematics. Input voltage variations to the amplifier of the tendons will maintain required length of each tendon to achieve the requested angle between the platforms. These are then understood geometrically to estimate the possible workspace.

*1.1. Research on Tendon-Based Parallel Manipulator.* For up to 20 years, research has continued on parallel robots, and today many, especially the planar parallel manipulators, have found their way into practical applications such as positioning devices, motion generators, and ultrafast pick and place robots [1]. Perhaps the most well-known and widely used of these parallel robots is the Stewart platform, which gained prominence due to its use in flight simulators. The traditional Stewart platform actuated by pistons attached to the base and

the platform by universal or ball-and-socket joints has given rise to other variations of such platforms. Of these variants those are of interest are firstly using compliant members and secondly using tendon or cable actuation.

In Korea, Choi et al. proposed the use of a passive compliant Stewart platform to accurately measure both position and force on each member of the platform [2]. Linear springs with encoders were placed in place of active pistons to determine the position and forces on the master robot to be mimicked by the slave. Though the compliant members were not used as active actuators, their use in Stewart platform opens up new grounds. Moon and Kota took this concept and applied it to active members [3]. They added compliant joints to piston-like linear actuators and incorporated a central constraining leg when fewer than 6 DOFs were required.

The idea of the constraining central leg introduces another method of configuring the Stewart platform. In the area of tendon-driven or cable-suspended platforms, few configurations have been proposed. The best known cable-suspended planar parallel robots are the RoboCranes developed at NIST [4, 5], where the end-effector sits on a platform suspended from a fixed frame using 6 cables to achieve 6 DOFs. Issues regarding the workspace and design of general cable-based planar robots were addressed by Fattah and Agrawal [6], where the platform was not only suspended but also constrained by cable from above and below. A tendon can provide some amount of load and, to assure that the tendon is always under tension, different solutions are advised. Sometimes the end-effector is suspended from the tendons and, by use of the gravity force or any other passive force against the moving platform, this is ensured [7]. Another more applicable solution for high acceleration applications is to use redundant actuators and to resolve the redundancy to ensure positive tension in all the tendons. This can be performed in a fully constrained or overconstrained moving platform [8], but with more difficulties to analyze the geometry [9] or force and possible workspace [10, 11].

#### *Tendon-Based Parallel Manipulator Application*

(1) *RoboCrane*. NIST implemented RoboCrane to carry on a series of applications such as assembly, lifting, spraying, and building structures [12]. Also, NIST worked on some theoretical analysis of kinematic modelling, stiffness, and workspace issues for the cable robot. The results concluded that the design neglected the weight of the cable; thus the stiffness of this robot depends on cable stiffness, the position of end-effectors, and the mass of the lifting load.

(2) *FALCON-7*. FALCON project is implemented in Japan with cable-driven parallel robots as a supersonic robot [13]. Furthermore, a 7-cable 6-DOF cable-driven parallel manipulator was analyzed in their case study concerning modelling method and workspace calculation. It is also worth noting that the dynamic performance can be improved by increasing tensions based on the relationship of stiffness and tension in this kind of cable robot and it is verified experimentally [13].

(3) *SACSO Wind-Tunnel Model*. SACSO was developed as another application of cable-driven parallel manipulators by ONERA, France, which is a 9-cable parallel robot [14]. In this study, the types and functionality of cable-driven parallel robots are discussed and a kinematic cable-driven parallel manipulator is presented. Besides, investigations regarding tension and dynamic characteristics are also taken in [14].

(4) *SEGESTA Experimental Platform*. Some researchers in Duisburg-Essen University of Germany built SEGESTA, a cable robot. Researchers used this platform to study the kinematic modelling, workspace calculation method, instant tension distribution, and trajectory planning issues [15].

(5) *SMA Actuated Cable-Driven Parallel Manipulator*. Shape memory alloy (SMA) actuator is a potential advanced component for servo systems of aerospace vehicles and aircraft. SMA triple wires perform two degrees of freedom (DOFs) connected with a joint where the mobility range close to  $\pm 60^\circ$  in the research [16]. The fuzzy proportional-integral-derivative (PID-) controlled actuator drive was designed using antagonistic SMA triple wires. This research showed the investigation of the external interference to the system proved the controllable maximum output [16].

## **2. Modeling of Smart Actuator**

A smart material-based actuator model is proposed here to develop a flexible manipulator. Investigation of the kinematic and dynamic feasibility of the actuator is taken into account in this research. Considering the advantages of the compliant members and that of the tendon-actuated planar parallel mechanisms, a design is suggested here where both the compliant aspect and tendon actuation could be used to develop simple miniature Stewart platforms that could be used as linkable modules of a locomotion device.

2.1. *Proposed Model*. One of the more comprehensive of treatments given to tendon-driven Stewart platforms is that of Verhoeven et al. [17]. In their formulation, they divide such platforms into two major classes, the first being the “completely restrained positioning mechanism” (CRPM), where tendons are attached with the platforms like a compression spine. This makes perfect sense since tendons are only able to exert tensile forces and not compressive ones and therefore are paired into opposing sets, much like antagonistic muscles found in limbs of living organisms. However, another cable is necessary to balance forces and effective torques to maintain stable positions. In such situations the number of cables will always be one more than the desired DOF. Thus  $n+1$  wires are needed to actuate a platform of  $n$  DOFs. The second class of platforms is known as the “incompletely restrained positioning mechanism” (IRPM) where tendons are positioned only below or above the platform. In this configuration an external force must be added to reverse the tensile actuation of the wires. The most common example of such a force is gravity, as in the RoboCrane where the platform is suspended by cable attached to fixed points above it. In this configuration, as the wire is relaxed or released, the weight of the platform

will force it to traverse to the desired position. Since gravity acts vertically in the  $-z$ -direction, it does not generate torque about  $z$  and hence an extra cable is not necessary to stabilize the platform, allowing  $n$  cables to produce  $n$  DOF [18, 19].

The proposed design, here, also falls into the IRPM but, rather than relying on gravity to provide the external force, a compliant member is added to maintain the external force at any orientation. While the RoboCrane can only function with cable above the platform, the new configuration will allow the platform to operate with cables below it, much like the traditional Stewart platform.

In the proposed Stewart platform, both the upper and lower platforms are of configurations of equilateral triangles with cables attached close to the vertices. One cable attaches each of the vertices of the lower platform to the vertices directly above it on the upper platform. The three tendons thus enable the platform to exhibit 3 DOFs. In order for the upper end-effector platform not to collapse onto the fixed base platform, a compliant central column must be added. The joint between the column and the upper platform as well as with the lower platform is fixed. The central column therefore at the point of attachment with the platform will always form a right angle regardless of orientation. Moments and forces are transferred into the column at both ends; hence the column can be modeled as a cantilever beam with moment and force acting upon the free end. Furthermore, the column needs to be able to compress upon itself and bend in the desired direction to achieve 3 DOFs. If the column were to bend only, then only 2 DOFs are achievable. Thus, a spring of a fairly large diameter is proposed as the central support. The spring is able to undergo compression and bending, and the large diameter will prevent the spring from buckling out of position when a bending force is applied together with compression. With this configuration, the three tendons can be actuated independently to achieve the desired position of the end-effector.

In this application, however, due to the nature of the 3-DOF device, position actually determines the orientation rather than the exact Cartesian position of the end-effector. The interest in this situation is the angular displacement of the upper platform with respect to the lower one. The desired output of the system therefore is the angle between the upper and lower platform. When linked to one after another of such module it is the angle that will allow the chain of platforms to bend in different formation to achieve locomotion. For the output, therefore, three generalized coordinates are selected. The first is the height of the central column,  $h$ , effectively a translation along  $z$ , which can be compressed by applying tension on all three tendons as shown in Figure 1. The second and third coordinates are the angles formed by the upper platform and the lower platform about the  $x$ - and  $y$ -axes. Rather than composing this angle from rotations around  $x$  and  $y$ , spherical-like coordinates are adopted as shown in Figure 2. That is, in the  $x$ - $y$ -plane, angle  $\theta$  denotes the anticlockwise angle measured from the positive  $x$ -axis. The projection of the bent central column onto the  $x$ - $y$ -plane is therefore assigned the variable  $d$ . The second angle  $\varphi$  thus denotes the angle between the plane of the upper platform and  $d$ . This angle differs from the equivalent spherical coordinate, as the vertex

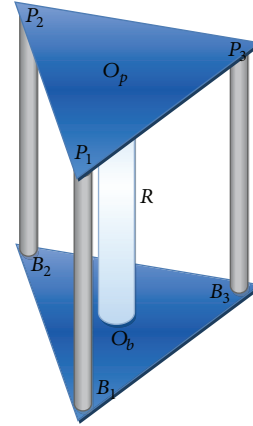


FIGURE 1: Proposed model configuration.

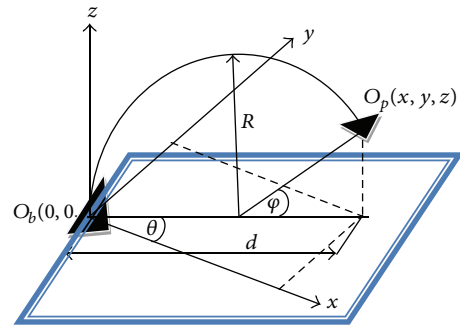


FIGURE 2: Proposed model bending geometry.

of this angle is not at the origin. In fact, the vertex of the angle moves further away from the origin as the angle decreases and comes closer as it increases.

Given the coordinates of  $h$ ,  $\theta$ , and  $\varphi$  in Figure 2, the Cartesian coordinates  $x$ ,  $y$ , and  $z$  can be determined, which then are in turn used to calculate the length of the three cables. Before performing the inverse kinematics assumptions are made in order to simplify the calculations. The assumption made here is that, for any desired position of the end-effector, the central column shall always bend to assume a circular arc of radius of curvature  $R$ . Though the column may not necessarily form a circular arc, this assumption is made as an approximation. The validity of this assumption shall be investigated upon constructing a physical model.

**2.2. Inverse Kinematics.** For every position of end-effector, precise lengths of each of the tendons must be given. Since both the lower and upper platforms have three points of attachment, the length from one point on the lower platform to another on the upper platform can be determined by taking the norm of the vector. To simplify the vector calculations, reference points are introduced: one on the center of the base,  $O_b$  and one on the center of upper platform  $O_p$ , which is also designated as the reference of the end-effector. The points where the tendons are attached on the base are then  $B_1$ ,  $B_2$ , and  $B_3$ , and due to their position at the vertices of a triangle which can be thought of as lying exactly within a circle of

radius  $r$ , their position vectors with respect to  $O_b$  would be given as

$$\begin{aligned} B_1 &= \begin{bmatrix} 0 \\ r \\ 0 \end{bmatrix}, & B_2 &= \begin{bmatrix} r \cos 30^\circ \\ -r \sin 30^\circ \\ 0 \end{bmatrix}, \\ B_3 &= \begin{bmatrix} -r \cos 30^\circ \\ -r \sin 30^\circ \\ 0 \end{bmatrix}. \end{aligned} \quad (1)$$

Similarly the points on the upper platform with respect to  $O_p$  would be

$$\begin{aligned} P_1 &= \begin{bmatrix} 0 \\ r \\ 0 \end{bmatrix}, & P_2 &= \begin{bmatrix} r \cos 30^\circ \\ -r \sin 30^\circ \\ 0 \end{bmatrix}, \\ P_3 &= \begin{bmatrix} -r \cos 30^\circ \\ -r \sin 30^\circ \\ 0 \end{bmatrix}. \end{aligned} \quad (2)$$

Before continuing further with the determination of cable lengths, the transformation from one set of coordinates to another must be delineated. From the coordinates determined earlier as  $h$ ,  $\theta$ , and  $\varphi$ , the first value that must be calculated is that of the radius of curvature,  $R$ , of the central spring, given by

$$R = \frac{180h}{\pi\theta}. \quad (3)$$

Then the coordinate  $(x, y, z)$  is determined to be

$$\begin{aligned} x &= R(1 - \cos \varphi) \sin \theta, \\ y &= R(1 - \cos \varphi) \cos \theta, \\ z &= R \sin \varphi. \end{aligned} \quad (4)$$

As for the positioning mechanism, in order to determine the vector from  $B_1$  to  $P_1$ , for example, when the end-effector is positioned at  $[x, y, z]^T$ , the vectors equation becomes

$$\overrightarrow{B_1P_1} = -\overrightarrow{B_1} + \overrightarrow{O_bO_p} + \overrightarrow{P_1} \quad (5)$$

which, in column vector form, would be

$$\overrightarrow{B_1P_1} = \begin{bmatrix} 0 \\ -r \\ 0 \end{bmatrix} + \begin{bmatrix} x \\ y \\ z \end{bmatrix} + \begin{bmatrix} 0 \\ r \\ 0 \end{bmatrix}. \quad (6)$$

The orientation of the upper platform must be broken down into roll, pitch, and yaw angles. Clearly as there is no rotation about  $z$  in this application, only the pitch and the yaw angles must be determined from the input coordinates of  $\theta$  and  $\varphi$ . Assigning  $\alpha$  as rotation about  $x$  and  $\beta$  as rotation about  $y$ , the following is calculated:

$$\begin{aligned} \alpha &= \tan^{-1} \left( \frac{\tan \varphi}{\sin \theta} \right), \\ \beta &= \tan^{-1} \left( \frac{\tan \varphi}{\cos \theta} \right). \end{aligned} \quad (7)$$

Using angles  $\alpha$  and  $\beta$ , the transformed position vectors on the platform would be given by

$$P_t = \begin{bmatrix} \cos \beta & \sin \alpha \sin \beta & \cos \alpha \sin \beta \\ 0 & \cos \alpha & -\sin \alpha \\ -\sin \beta & \sin \alpha \cos \beta & \cos \alpha \cos \beta \end{bmatrix} P_i. \quad (8)$$

For any position and orientation, then, the lengths are given by

$$l_1 = \|\overrightarrow{B_1P_1}\|, \quad l_2 = \|\overrightarrow{B_2P_2}\|, \quad l_3 = \|\overrightarrow{B_3P_3}\|. \quad (9)$$

Deriving the values for  $l_1$  completely, consider

$$\begin{aligned} l_1 &= \left\| \begin{bmatrix} 0 \\ -r \\ 0 \end{bmatrix} + \begin{bmatrix} x \\ y \\ z \end{bmatrix} \right. \\ &\quad \left. + \begin{bmatrix} \cos \beta & \sin \alpha \sin \beta & \cos \alpha \sin \beta \\ 0 & \cos \alpha & -\sin \alpha \\ -\sin \beta & \sin \alpha \cos \beta & \cos \alpha \cos \beta \end{bmatrix} \begin{bmatrix} 0 \\ r \\ 0 \end{bmatrix} \right\| \end{aligned} \quad (10)$$

or

$$\begin{aligned} l_1 &= \left( [r \sin \alpha \sin \beta + x]^2 + [r \cos \alpha - r + y]^2 \right. \\ &\quad \left. + [r \sin \alpha \cos \beta + z]^2 \right)^{1/2}. \end{aligned} \quad (11)$$

Similarly,  $l_2$  and  $l_3$  can be determined by

$$\begin{aligned} l_2 &= \left( [-r \cos 30 + x + r \cos \beta \cos 30 - r \sin \alpha \sin \beta \sin 30]^2 \right. \\ &\quad \left. + [r \sin 30 + y - r \cos \alpha \sin 30]^2 \right. \\ &\quad \left. + [z - r \sin \beta \cos 30 - r \sin \alpha \cos \beta \sin 30]^2 \right)^{1/2}, \\ l_3 &= \left( [-r \cos 30 + x + r \cos \beta \cos 30 - r \sin \alpha \sin \beta \sin 30]^2 \right. \\ &\quad \left. + [r \sin 30 + y - r \cos \alpha \sin 30]^2 \right. \\ &\quad \left. + [z - r \sin \beta \cos 30 - r \sin \alpha \cos \beta \sin 30]^2 \right)^{1/2}. \end{aligned} \quad (12)$$

The same can be repeated for  $l_2$  and  $l_3$ . Then adjusting each of the cables to the calculated lengths would result in the desired position of the end-effector. Figures 3 and 4 show the simulated result for different configuration of the upper platform.

**2.3. Dynamic Analysis of the Actuator.** In order to develop the dynamic model of the robot, the Lagrange-Euler method

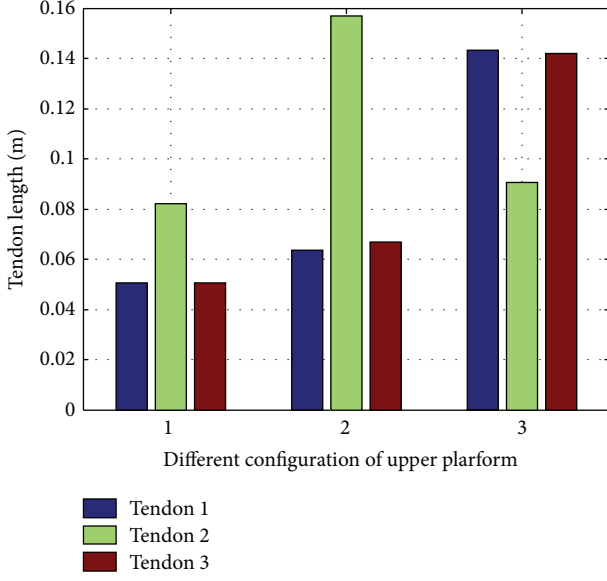


FIGURE 3: Lengths of the 3 tendons for different configuration. Tendons length versus different configuration of upper platform.

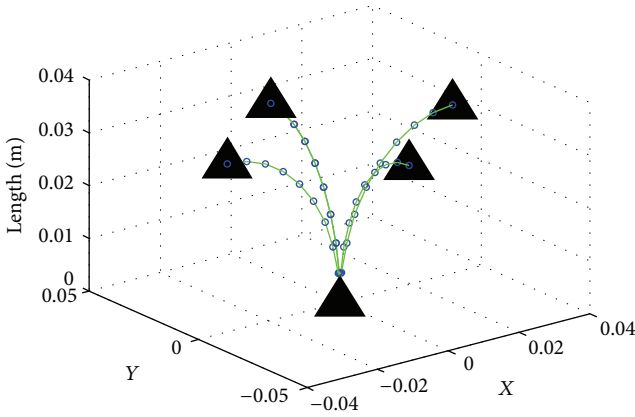


FIGURE 4: Shape of the central beam in different configuration.

is used. The simplified version of Lagrange-Euler equation is presented by

$$\sum_{j=1}^n M_{ij} \ddot{q}_j + C_i(\dot{q}, q) - \frac{\partial U(q)}{\partial q_i} + \frac{\partial f_c}{\partial \dot{q}_i} = Q_i, \quad 1 \leq i \leq n, \quad (13)$$

where  $q_i$  is the generalized coordinates,  $Q_i$  is the generalized force corresponding to  $q_i$ ,  $M$  is the inertia matrix,  $C_i$  the centrifugal and the coriolis matrix,  $U$  is the potential energy, and  $f_c$  is Rayleigh's dissipation function.

Figure 5 shows that forces  $f_{j1}$  and  $f_{j2}$  are applied by the actuator (with respect to spine), located between ribs AB and

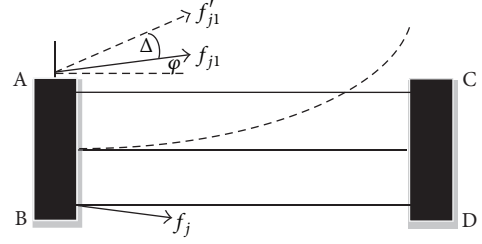


FIGURE 5: Approximate manipulator workspace.

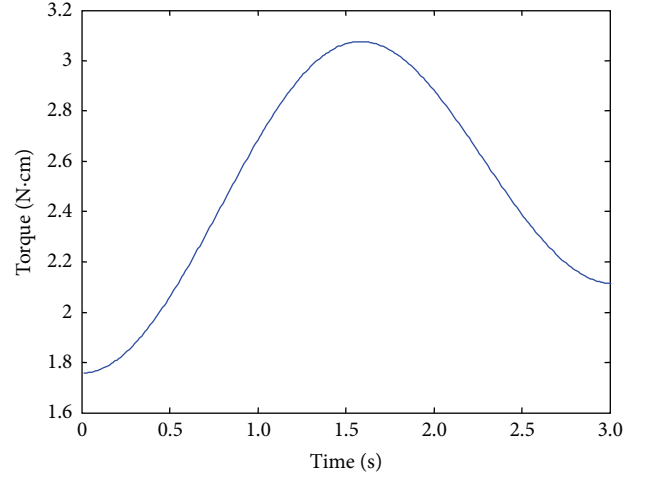


FIGURE 6: Torque profile of the single actuator.

TABLE I: EAP mechanical characteristics.

Variable	Value
$\rho p$ (density of electrode, $\text{Kg/m}^3$ )	21500
$\rho g$ (density of EAP, $\text{Kg/m}^3$ )	2600
$L$ (length of the EAP actuator, m)	0.040
$b$ (width of the EAP actuator, m)	0.020
$hb$ (thickness, m)	0.010
$E_b$ (Young's modulus of elasticity for EAP, Pa)	$3 \times 10^6$

CD. Based on Figure 12, the following relations are valid for forces  $f_{j1}$  and  $f_{j2}$  components along the  $x$ - and  $y$ -axes:

$$\begin{aligned} F_{j1x} &= f_{j1} \cos(\varphi_i + \Delta\varphi_i), \\ F_{j1y} &= f_{j1} \sin(\varphi_i + \Delta\varphi_i), \\ F_{j2x} &= f_{j2} \cos(-\varphi_i + \Delta\varphi_i), \\ F_{j2y} &= f_{j2} \sin(-\varphi_i + \Delta\varphi_i). \end{aligned} \quad (14)$$

Figure 6 shows the maximum torque value reaches at time 1.5~2 sec. The actuator has the largest torque value about 3.08 N-cm.

2.4. Modeling and Simulation of Smart (EAP) Actuator. The mechanical parameters of the EAP are shown in Table 1. The width of EAP is assumed to be 0.020 m. The blocking

TABLE 2: EAP electrical parameters.

Variable	Value
$R$ ( $\Omega$ )	78
$C$ (F)	$1.382e - 2$
$\tau Q$ (RC), sec	0.0106

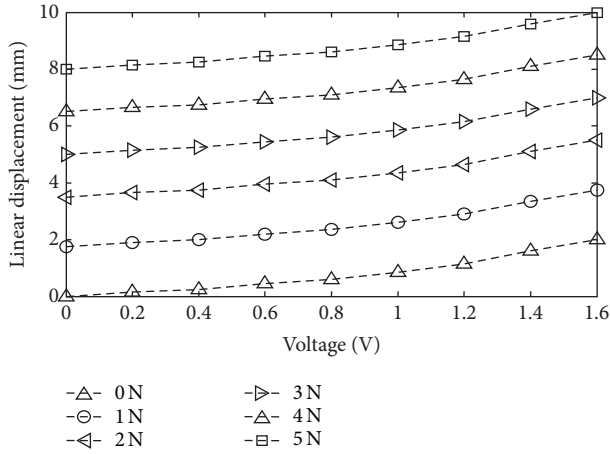


FIGURE 7: Voltage-elongation and force-elongation relationships of the EAP actuator.

force is measured by positioning a force sensor at the tip of an EAP actuator. The electrical parameters obtained from system identification procedure are shown in Table 2.

An experiment has been conducted to investigate the properties of a system driven by EAP. One of the EAP rolls is fixed to the base frame. On the other side, it is connected through stainless steel tendons to a pulley which moves a metallic bar. The EAP has thus the functionality of a muscle, whose levels of activation control the angular position of the joint. The actuation properties of the employed EAP roll is completely described in terms of developed stress and strain as a function of the applied voltage as shown Figure 7. In this framework, the controller is responsible of actuating the actuator and the elongation of the tendon. In order to measure the cable forces, force sensor is used and placed on the tendons.

### 2.5. Design and Fabrication of EAP-Based Flexible Actuator

**2.5.1. Solid Model of the Actuator.** The actuator of a single link contains two bases, three EAP tendons, and one spring-like soft material as shown in Figure 8. Figure 9 shows the top view of the actuator, where the three tendons are able to perform 3-DOF motion by the linearly tension-compression actuation of the tendons.

**2.5.2. Fabrication of the Actuator.** The EAP-based flexible actuator used in this research is shown in Figure 10. It consists of flexible central body and three EAP tendons are attached for tendon-driven Stewart platforms actuator. The actuator is



FIGURE 8: Perspective view of the 3D solid model of the actuator.

TABLE 3: Actuator dimensions and parameters.

Variable	Value
$L$ (length, m)	0.050
$D$ (diameter, m)	0.020
$m$ (mass, kg)	0.010

powered externally. The actuator's dimension and parameters are given in Table 3.

The parameters of the prototype as shown in Figure 10 are stated in the Table 3. The initial length of each of the EAP tendons is 50 cm. The fixed diameter of the platform is 20 cm and the total mass of the actuator is 10 gm.

In order to provide safety to the user, the EAP actuator was mounted inside a transparent rubber pocket. Three EAP tendons were attached between two platforms. This actuator performs 3-DOF motion.

## 3. Singularities of the Proposed Mechanism

Though the inverse kinematics of a parallel robot is relatively straightforward compared to serial mechanisms, the definition of the Jacobian requires a more complex method. Traditionally, the understanding of parallel robot singularities requires the formulation of two Jacobian matrices, both of which are derived from the implicit function joint parameters and end-effector coordinates. This function is obtained from the kinematic constraints of the manipulator:

$$f(x, q) = 0, \quad (15)$$

where  $q$  is the set of input coordinates and  $x$  is the output. Differentiating the implicit function, we get

$$J_x \cdot \dot{X} = J_q \cdot \dot{q}, \quad (16)$$

from which both Jacobians are deduced:

$$J_x = \frac{\partial f}{\partial x}, \quad (17)$$

$$J_q = -\frac{\partial f}{\partial q}.$$

For fully parallel mechanisms, such as the proposed design, the final relationship can be written as

$$\dot{q} = J_q^{-1} \cdot J_x \cdot \dot{X}. \quad (18)$$

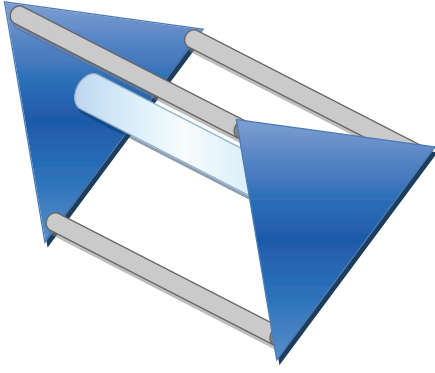


FIGURE 9: Top view of the actuator.



FIGURE 10: Prototype of the EAP-based flexible actuator.

In Figure 11, the mechanism, therefore, will be in a singular position if either of the two or both Jacobians are singular. For the present design, the implicit functions are determined by the kinematic loops found in the mechanism; however, rather than solving for singularities in the 3D model, a 2D representation is adopted to simplify the calculations and be taken as a point of departure.

From the above configuration, the lengths of the two cables are resolved into its  $x$ - and  $y$ -components leading to the following equations:

$$\begin{aligned} f_1 &= (x + r - r \cos \theta)^2 + (y - r \sin \theta)^2 - q_1^2 = 0, \\ f_2 &= (x - r + r \cos \theta)^2 + (y + r \sin \theta)^2 - q_2^2 = 0. \end{aligned} \quad (19)$$

Taking partial derivatives of both functions, the following equations are obtained:

$$\frac{\partial f_1}{\partial x} = 2(x + r - r \cos \theta),$$

$$\frac{\partial f_1}{\partial y} = 2(y - r \sin \theta),$$

$$\frac{\partial f_1}{\partial \theta} = 2(x + r - r \cos \theta) r \sin \theta - 2(y - r \sin \theta) r \cos \theta,$$

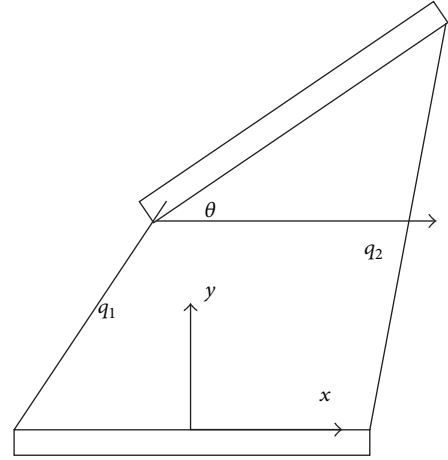


FIGURE 11: 2D representation of the model.

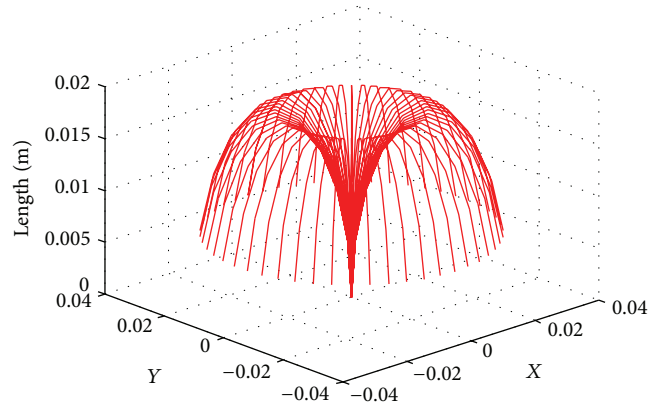


FIGURE 12: Approximate manipulator workspace.

$$\frac{\partial f_2}{\partial x} = 2(x - r + r \cos \theta),$$

$$\frac{\partial f_2}{\partial y} = 2(y + r \sin \theta),$$

$$\frac{\partial f_2}{\partial \theta} = -2(x - r + r \cos \theta) r \sin \theta + 2(y + r \sin \theta) r \cos \theta,$$

$$\frac{\partial f_1}{\partial q_1} = -2q_1,$$

$$\frac{\partial f_1}{\partial q_2} = 0,$$

$$\frac{\partial f_2}{\partial q_1} = 0,$$

$$\frac{\partial f_2}{\partial q_2} = -2q_2.$$

(20)

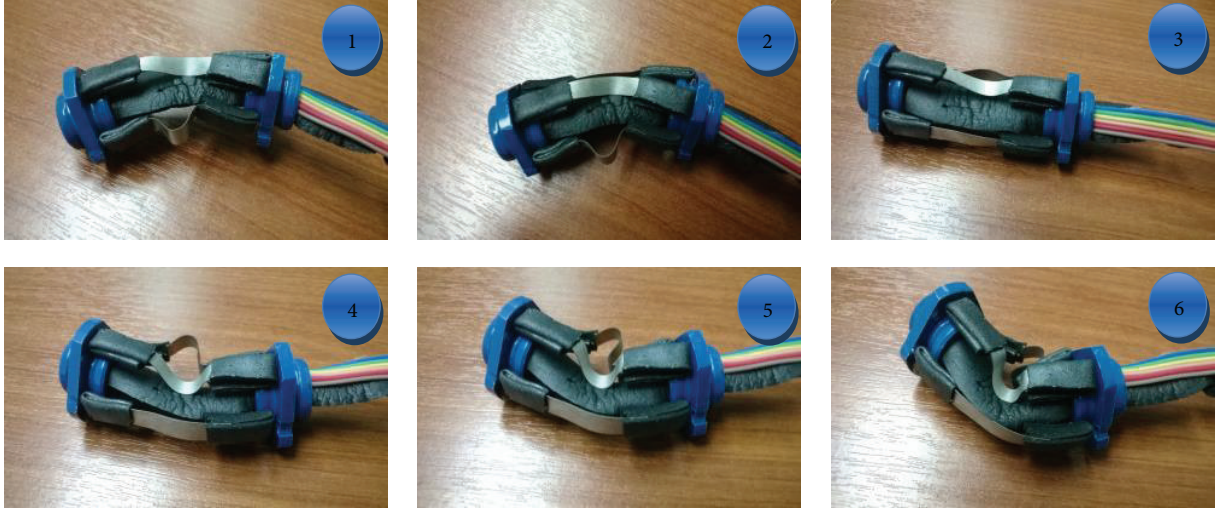


FIGURE 13: Prototype presents the actual process of actuator movement.

The Jacobians are thus defined as

$$J_x = \begin{bmatrix} 2(x+r-r\cos\theta) & 2(y-r\sin\theta) & 2(x+r-r\cos\theta)r\sin\theta - 2(y-r\sin\theta)r\cos\theta \\ 2(x-r+r\cos\theta) & 2(y+r\sin\theta) & -2(x-r+r\cos\theta)r\sin\theta + 2(y+r\sin\theta)r\cos\theta \\ 0 & 0 & 0 \end{bmatrix}, \quad (21)$$

$$J_q = \begin{bmatrix} -2q_1 & 0 \\ 0 & -2q_2 \end{bmatrix},$$

where the determinants would be expressed as

$$\begin{aligned} \det J_x &= 2(x+r-r\cos\theta) - 2(y-r\sin\theta) \\ &\quad + 2(x+r-r\cos\theta)r\sin\theta - 2(y-r\sin\theta)r\cos\theta, \\ \det J_q &= -4q_1q_2. \end{aligned} \quad (22)$$

Factorizing (15) and equating the determinants to zero gives

$$\begin{aligned} \cos\theta(-2r-2yr) + \sin\theta(2r+2r^2+2xr) \\ + 2r+2x-2y &= 0, \\ -4q_1q_2 &= 0. \end{aligned} \quad (23)$$

As for the lengths, it is obvious that the lengths can never be equal to zero. However, for other singularities, each angle will have its own set of singularities. When  $\theta$  is zero, that is, when the platform is parallel to the base, the end-effect cannot occupy the set of positions  $x$  and  $y$  given by the following linear equation:

$$y = \frac{1}{r+1}x. \quad (24)$$

Similarly when  $\theta$  is  $90^\circ$  the set of singularities is defined by

$$y = (r+1)x + 2r + r^2, \quad (25)$$

and when  $\theta$  is  $-90^\circ$  the equation concerned is

$$y = (1-r)x - r^2. \quad (26)$$

Though the above equations will give us the analytical singularities, it is more likely that the physical limitations of the manipulator will be encountered first.

Going back to the 3D model, there are numerous physical limits. The first is the maximum and minimum limits of the vertical compressible column in the  $z$ -direction. The second would be the limitations posed by the wires and the platforms. The wires can be shortened only up to the point where the edges of the platforms meet. Here the ration of the height of spring to the radius of the base becomes critical. If the spring is too long compared to the radius, the spring would bend too far so as to almost complete a circle. If the height is too short compared to the radius then the angle of deflection is limited. If a maximum of  $60^\circ$  deflection is desired in all directions then the desired  $h:r$  ration would be  $\pi:3$ .

Given these constraints, and taking linear approximations of a nonlinear model, the approximate workspace of the 3 DOFs is given below for a fixed height of 25 mm and radius of 24 mm is shown in Figure 12.

The center of the upper platform thus traverses a surface, and when the height of the central spring is increased or decreased, new surfaces are formed hence occupying a volume in space.

## 4. Experiment

An experimental setup has been carried out to demonstrate proposed design. The actuator that we used for the experiments is smart material actuated parallel platform as shown in Figure 10 [20]. In this experiment, the link represents the 3-DOF movement according to the proposed kinematic analysis. Figure 13 shows six angular displacements between two parallel plates attached at the two ends of the actuator against different voltages in different tendons.

If 3 tendons' lengths are the same, the central compliant column only shortens along the  $z$ -axis of the actuator and the top and bottom platforms remain approximately parallel. In the following step, adjustment of the lengths of the three tendons helps change the angular position of the actuator in a new location. Thus the actuator has a wide scope of 3D workspace. Furthermore the series of this parallel platform can be performed by snake-like robot navigation in search and rescue mission [21].

## 5. Conclusions

Smart material actuated tendon-based flexible actuator for 3D angular positioning is discussed in this research. The design and kinematic analysis of the actuator are also demonstrated in this work. In particular, this investigation focuses on the angular deflection of the upper platform with respect to the lower platform. A manipulator consisting of an IRPM mechanism that contains a compliant central column connected between two parallel platforms is capable of demonstrating angular displacement between the platforms. The angular displacement of  $30^\circ$  between the platforms was achieved experimentally. It was also found that the curvature of the central compliant column assumes approximately a shape of a circular arc within this  $30^\circ$  angular deformation.

## Conflict of Interests

The authors declare that there is no conflict of interests regarding the publication of this paper.

## References

- [1] J.-P. Merlet, "Still a long way to go on the road for parallel mechanisms," in *Proceedings of the ASME International Mechanical Engineering Congress and Exposition (IMECE '02)*, pp. 95–99, Montréal, Canada, 2002.
- [2] S. W. Choi, Y. J. Choi, and S. Kim, "Using a compliant wrist for a teleoperated robot," in *Proceedings of the IEEE/RSJ International Conference on Intelligent Robots and Systems (IROS '99)*, pp. 585–589, Los Alamitos, Calif, USA, 1999.
- [3] Y. M. Moon and S. Kota, "Design of compliant parallel kinematic machines," in *Proceedings of the ASME International Design Engineering Technical Conferences and Computers and Information in Engineering Conference*, pp. 35–41, American Society of Mechanical Engineers, 2002.
- [4] R. Bostelman, A. Jacoff, F. Proctor, T. Kramer, and A. Wavering, "Cable-based reconfigurable machines for large scale manufacturing," in *Proceedings of the Japan-USA Symposium on Flexible Automation*, pp. 23–26, July 2000.
- [5] R. Bostelman, J. Albus, N. Pagalakis, A. Jacoff, and J. L. Gross, "Applications of the NIST Robocrane," *Robotics and Manufacturing*, vol. 5, pp. 403–410, 1994.
- [6] A. Fattah and S. K. Agrawal, "Design of cable-suspended planar parallel robots for an optimal workspace," in *Proceedings of the Workshop on Fundamental Issues and Future Research Directions for Parallel Mechanisms and Manipulators*, pp. 195–202, Quebec City, Canada, October 2002.
- [7] H. D. Taghirad and M. Nahon, "Kinematic analysis of a macro-micro redundantly actuated parallel manipulator," *Advanced Robotics*, vol. 22, no. 6-7, pp. 657–687, 2008.
- [8] S. Oh and S. Agrawal, "Cable suspended planar robots with redundant cables: controllers with positive tensions," *IEEE/Transactions on Robotics*, vol. 21, no. 3, pp. 457–465, 2005.
- [9] M. M. Aref and H. D. Taghirad, "Geometrical workspace analysis of a cable-driven redundant parallel manipulator: KNTU CDRPM," in *Proceedings of the IEEE/RSJ International Conference on Intelligent Robots and Systems (IROS '08)*, pp. 1958–1963, September 2008.
- [10] A. Z. Loloie, M. M. Aref, and H. D. Taghirad, "Force feasible workspace analysis of cable-driven parallel manipulators using LMI approach," in *Proceedings of the IEEE/ASME International Conference on Advanced Intelligent Mechatronics (AIM '09)*, pp. 1034–1039, July 2009.
- [11] I. Mordatch, E. Todorov, and Z. Popović, "Discovery of complex behaviors through contact-invariant optimization," *ACM Transactions on Graphics—Proceedings of ACM SIGGRAPH*, vol. 31, no. 4, article 43, 2012.
- [12] A. M. Lytle, K. S. Saidi, R. V. Bostelman, W. C. Stone, and N. A. Scott, "Adapting a teleoperated device for autonomous control using three-dimensional positioning sensors: experiences with the NIST RoboCrane," *Automation in Construction*, vol. 13, no. 1, pp. 101–118, 2004.
- [13] S. Kawamura, H. Kino, and C. Won, "High-speed manipulation by using parallel wire-driven robots," *Robotica*, vol. 18, no. 1, pp. 13–21, 2000.
- [14] Y.-Q. Zheng, "Force-measuring experiment for the scale model of WDPSS in low-speed wind tunnel," *Journal of Huaqiao University (Natural Science)*, no. 2, pp. 119–122, 2009.
- [15] L. Mikelsons, T. Bruckmann, M. Hiller, and D. Schramm, "A real-time capable force calculation algorithm for redundant tendon-based parallel manipulators," in *Proceedings of the IEEE International Conference on Robotics and Automation (ICRA '08)*, pp. 3869–3874, May 2008.
- [16] Z. Shi, T. Wang, D. Liu, C. Ma, and X. Yuan, "A fuzzy PID-controlled SMA actuator for a two-DOF joint," *Chinese Journal of Aeronautics*, vol. 27, no. 2, pp. 453–460, 2014.
- [17] R. Verhoeven, M. Hiller, and S. Takodoro, "Workspace of tendon-driven Stewart platforms: basics, classification, details on the planar 2-dof class," in *Proceedings of the 4th International Conference on Motion and Vibration Control*, ETH Zurich, Zurich, Switzerland, August 1998.
- [18] N. Simaan and M. Shoham, "Geometric interpretation of the derivatives of parallel robots' Jacobian matrix with application to stiffness control," *Journal of Mechanical Design*, vol. 125, no. 1, pp. 33–42, 2003.
- [19] A. M. Hay and J. A. Snyman, "The chord method for the determination of nonconvex workspaces of planar parallel manipulators," *Computers & Mathematics with Applications*, vol. 43, no. 8-9, pp. 1135–1151, 2002.

- [20] M. M. Billah, R. Khan, and A. A. Shafie, "Modeling of the smart material actuated robotic snake I (SMARS-I)," *Journal of Engineering Design*. In press.
- [21] M. M. Billah, M. Ahmed, and S. Farhana, "Walking hexapod robot in disaster recovery: developing algorithm for terrain negotiation and navigation," *Proceedings of World Academy of Science, Engineering and Technology*, vol. 42, pp. 328–333, 2008.



**Hindawi**

Submit your manuscripts at  
<http://www.hindawi.com>

